NONLINEAR SOIL-STRUCTURE INTERACTION ANALYSIS USING DYNAMIC FLEXIBILITY OF SOIL FOR IMPULSE FORCES

J.P. Wolf (I)
P. Obernhuber (I)
Presenting Author: J.P. Wolf

SUMMARY

A rigorous procedure to calculate soil-structure interaction for a nonlinear structure and a linear unbounded soil is discussed. The dynamic-flexibility coefficients for unit impulse forces of the horizontally layered halfspace are determined. By way of illustration, a structure with a nonlinear base isolation and a structure with partial uplift of its basemat are analyzed.

INTRODUCTION

The procedures to analyze soil-structure interaction for a linear system are well developed (Ref. 1). The calculation is normally performed in the frequency domain, whereby the (frequency-dependent) dynamic stiffness of the soil takes the radiation condition of the unbounded domain into account. It is, however, well known that structures are designed by providing sufficient ductility to perform in the nonlinear range for high seismic excitation. Base-isolation systems with friction plates, which exhibit strong nonlinear characteristics for the design-basis earthquake are routinely used, even for nuclear-power plants. Other local nonlinear effects include the partial uplift of the basemat, the separation occurring between the walls of the base and the neighboring soil in the case of embedded structures, and the highly nonlinear soil behavior arising adjacent to the basemat. In all these cases, the nonlinear behavior is restricted to the structure and possibly an irregular soil region adjacent to the structure (the near field), while the far field of the unbounded soil is assumed to remain linearly visco-elastic. Referring to Fig. 1, the line joining the nodes with subscript b (for base) separates these two regions. The subscript s (for structure) denotes the nodes of the nonlinear discretized system. To analyze such cases, procedures which work directly in the time domain have to be used.

The basic equation of motion in the time domain is formulated as (Ref.2)

$$\begin{bmatrix} [M_{ss}] & [M_{sb}] \\ [M_{bs}] & [M_{bb}] \end{bmatrix} \begin{Bmatrix} \{\ddot{u}_s^t(t)\} \\ \{\ddot{u}_b^t(t)\} \end{Bmatrix} + \begin{Bmatrix} \{P_s(t)\} \\ \{P_b(t)\} \end{Bmatrix} + \begin{Bmatrix} \{0\} \\ \int_0^t [S_{bb}^g(t-\tau)]\{u_b^t(\tau)\}d\tau \end{Bmatrix} = \begin{Bmatrix} \{0\} \\ \int_0^t [S_{bb}^g(t-\tau)]\{u_b^g(\tau)\}d\tau \end{Bmatrix} \quad (1)$$

$[M]$ is the mass matrix, $\{u^t\}$ denotes the vector of the total displacements, $\{P\}$ the vector of the (nonlinear) internal forces, $\{u_b^g\}$ the vector of the scattered motion, which follows from the free-field response of the site (Ref. 1), and the dynamic-stiffness matrix of the soil, taking the excavation into account in the time domain $[S_{bb}^g(t)]$, contains the forces required to produce unit-impulse displacements. The Eq. 1 contains convolution integrals and can

(I) Structural Engineer, Electrowatt Engineering Services Ltd.,
P.O. Box CH-8022 Zürich, Switzerland

be solved e.g. by explicit integration.

Approximate expressions for the dynamic-stiffness coefficients in the time domain of a rigid circular basemat resting on the surface of an elastic half-space are discussed in Ref. 3.

INTRODUCTORY EXAMPLE

For the purpose of studying the properties of the dynamic stiffness in the time domain, the semi-infinite rod with an exponentially increasing area

$$A(z) = A_o \exp(z/f) \tag{2}$$

is examined (Fig. 2). A_o represents the area at $z = 0$, f is a parameter. In the frequency domain, the dynamic-stiffness coefficient $S(a_o)$ at $z = 0$ can be expressed as (Ref. 4)

$$S(a_o) = EA_o(1+\sqrt{1-4a_o^2})/(2f) \tag{3}$$

with the dimensionless frequency a_o defined as

$$a_o = \omega f/c_o \tag{4}$$

with $c_o = \sqrt{E/\rho}$ (E = modulus of elasticity, ρ = mass density). In the time domain, the dynamic-stiffness coefficient $S(\bar{t})$ (force for unit-impulse displacement) follows from the Fourier transformation

$$S(\bar{t}) = \frac{c_o}{2\pi f}\int_{-\infty}^{+\infty} S(a_o)\exp(ia_o\bar{t})da_o \tag{5}$$

with the dimensionless time $\bar{t}$ defined as

$$\bar{t} = \frac{c_o}{f}t \tag{6}$$

As the frequency tends to infinity, $S(a_o)$ will approach infinity. It is thus necessary to decompose $S(a_o)$ into a regular part and a singular part whose transformation is valid only in the sense of a distribution. Substituting Eq.3 in Eq.5 leads to

$$S(\bar{t}) = \frac{c_o EA_o}{f^2}\left[\frac{1}{2\pi}\int_{-\infty}^{+\infty}\frac{1}{2}\exp(ia_o\bar{t})da_o + \frac{1}{2\pi}\int_{-\infty}^{+\infty}\frac{\sqrt{1-4a_o^2}}{2}\exp(ia_o\bar{t})da_o\right] \tag{7}$$

The first term within the bracket is equal to $\delta(\bar{t})/2$ (Dirac delta function). For $\bar{t} > 0$, the second term can be shown to result in $J_1(\bar{t}/2)/(2\bar{t})$, where J_1 is the Bessel function of the first kind and of the first order. The remaining contribution of the second term leads to $d\delta(\bar{t})/d\bar{t}$. Eq. 7 is thus transformed to (for $\bar{t} \geq 0$)

$$S(\bar{t}) = \frac{c_o EA_o}{f^2}\left[\frac{1}{2}\delta(\bar{t}) + \frac{d\delta(\bar{t})}{d\bar{t}} + \frac{1}{2\bar{t}}J_1(\frac{\bar{t}}{2})\right] \tag{8}$$

and for $\bar{t} < 0$, $S(\bar{t}) = 0$.

The force R(t) follows from the convolution integral of S(t) and the displacement w(t).

$$R(t) = \int_o^t S(t-\tau)\, w(\tau)d\tau \tag{9}$$

Substituting Eq. 8 and with $\delta(\bar{t}) = \delta(t)f/c_o$ and $d\delta(\bar{t})/d\bar{t} = \dot{\delta}(t)f^2/c_o^2$, Eq. 9

results in

$$R(t) = \frac{EA_o}{f}\left[\frac{1}{2}\,w(t) + \frac{f}{c_o}\,\dot{w}(t) + \frac{1}{2}\int_o^t \frac{1}{t-\tau}\,J_1\left(\frac{c_o}{2f}(t-\tau)\right)w(\tau)\,d\tau\right] \tag{10}$$

The first term can be interpreted as a spring with a coefficient $EA_o/(2f)$ (which is half the static stiffness), the second as a viscous damper with a coefficient EA_o/c_o.

As the dynamic-flexibility coefficient $F(a_o) = 1/S(a_o)$ tends to zero for $\omega \to \infty$, working with dynamic flexibilities may turn out to be computationally simpler. In the time domain,

$$F(\bar{t}) = \frac{c_o}{2\pi f}\int_{-\infty}^{+\infty}(1/S(a_o))\,\exp(ia_o\bar{t})\,da_o \tag{11}$$

results. $F(\bar{t})$ multiplied by $f^2/(c_o EA_o)$ is plotted in Fig. 3 as a solid line. Since no singular part exists, the integral in Eq. 11 can be calculated directly, using the Fast Fourier Transform. As the dynamic-flexibility coefficient in the time domain equals the displacement for a unit-impulse force, the displacement w(t) follows as

$$w(t) = \int_o^t F(t-\tau)\,R(\tau)\,d\tau \tag{12}$$

Viscous-material damping can be introduced as

$$E^* = E(1+2\bar{\zeta}_v a_o i) \tag{13}$$

whereby the non-dimensionalized damping ratio

$$\bar{\zeta}_v = \frac{c_o}{f}\,\zeta_v \tag{14}$$

applies. The corresponding dynamic-flexibility coefficient $F(\bar{t})$ is also shown as a dashed line for $\bar{\zeta}_v = 0.2$ in Fig. 3. In contrast to the undamped case, $F(\bar{t} = 0^+) = 0$ for the viscously damped one.

LAYERED HALFSPACE

For surface and embedded (two- and three-dimensional) foundations, the dynamic-stiffness coefficients $S(a_o)$ in the frequency domain are routinely determined (Refs. 5, 6). The soil is assumed as a horizontally layered viscoelastic halfspace. The structure-soil interface is discretized with boundary elements. The source loads and the corresponding displacements and surface tractions are expanded in the wave-number domain using Fourier and Bessel functions for the two- and three-dimensional cases, respectively. As the number of boundary elements is limited, the accuracy for higher frequencies diminishes. However, analytical solutions exist for the asymptotic behavior ($\omega \to \infty$)(Ref.7).

The Fourier transform of $1/S(a_o)$ leads to the dynamic-flexibility coefficient in the time domain $F(\bar{t})$, i.e. the displacement caused by a unit-impulse force

$$F(\bar{t}) = \frac{c_s}{2\pi a}\int_{-\infty}^{+\infty}\frac{1}{S(a_o)}\,\exp(ia_o\bar{t})\,da_o \tag{15}$$

with

$$a_o = \frac{\omega a}{c_s} \tag{16}$$

$$\bar{t} = \frac{c_s}{a}\,t \tag{17}$$

where a_o and $\bar{t}$ are the dimensionless frequency and time, respectively. c_s denotes the shear-wave velocity, and a the characteristic length, e.g. the radius. The integration is performed numerically up to that a_o for which the analytical high-frequency solution starts to be valid. This limit determines the mesh size of the boundary elements. The remaining part of the integral can be expressed in closed form.

The dynamic-flexibility coefficients in the time domain for the horizontal, vertical and rocking degrees of freedom of a circular rigid disc resting on the surface of a layered halfspace are examined. The two limiting cases are presented: in Fig. 4 the coefficients $\bar{F}(\bar{t})$ "non-dimensionalized" by the static values (of the halfspace) specified in the captions for the homogeneous halfspace, and in Fig. 5 those for the layer with a depth equal to the radius a built-in at its base. Poisson's ratio ν equals 0.33. The dynamic-stiffness coefficients are taken from Ref. 5. Uniform viscous-material damping is also introduced, defined by

$$G^* = G(1+2\bar{\zeta}_v a_o i) \qquad (18) \qquad (\lambda+2G)^* = (\lambda+2G)(1+2\bar{\zeta}_v a_o i) \qquad (19)$$

whereby the non-dimensionalized damping ratio is defined as

$$\bar{\zeta}_v = \frac{c_s}{a}\,\zeta_v \qquad (20)$$

λ and G are the two Lamé constants. As is apparent, all flexibility coefficients are, from a practical point of view, equal to zero for $\bar{t} < 0$. For both the undamped halfspace and layer, $\bar{F}(\bar{t} = 0^+)$ can be calculated using one-dimensional wave theory. For the horizontal, vertical and rocking degrees of freedom, the values $8/(\pi(2-\nu))$, $2/(\pi(1-\nu))$ and $16/(3\pi(1-\nu))$, respectively, result. For the damped cases, $\bar{F}(\bar{t} = 0^+)$ equals zero, as the selected material law (Voigt model) exhibits no instantaneous elasticity. The early-time behavior of the flexibility of the halfspace and that of the layer are identical; in particular the maxima are the same. As expected, the oscillations are more pronounced for the layer and for small damping.

COMPUTATIONAL PROCEDURE

An analogous formulation to Eq. 1 can be derived, using a flexibility formulation for the contribution of the soil, together with the direct stiffness method for the structure and the irregular soil region. The contribution of the far field is formulated as

$$\{u_b^t(t)\} - \{u_b^g(t)\} = \int_o^t [F_{bb}^g(t-\tau)]\{R_b(\tau)\}\,d\tau \qquad (21)$$

where $\{R_b(\tau)\}$ denotes the vector of the interaction forces of the far field.

Starting from the known accelerations, velocities, and displacements of the far field up to time t, determined in n steps, the displacements at time $t + \Delta t$, $\{u^t\}_{t+\Delta t}$, are calculated with the central-difference method. Eq. 21 can then be solved for the unknown interaction forces $\{R_b\}_{t+\Delta t}$

$$\{R_b\}_{t+\Delta t} = [F_{bb}^g]_o^{-1}(\{u_b^t\}_{t+\Delta t} - \{u_b^g\}_{t+\Delta t} - \sum_{i=1}^{n} [F_{bb}^g]_{(n+1-i)\Delta t}\{R_b\}_{i\Delta t}) \qquad (22)$$

No inversion has to be performed, as $[F_{bb}^g]_o$ is a diagonal matrix. For a lumped mass matrix, the acceleration follows as

$$\{\ddot{u}^t_b\}_{t+\Delta t} = -[M_{bb}]^{-1}(\{P_b\}_{t+\Delta t} + \{R_b\}_{t+\Delta t}) \qquad (23)$$

STRUCTURE WITH BASE ISOLATION

The simple structure shown in Fig.6, with mass m with and without base isolation is investigated. 3/4 m is concentrated at the height h. The mass moment of inertia associated with the rocking degree of freedom at the rigid circular basemat of radius a equals 1/4 a^2m. For a structure with base isolation, half of the mass at the basemat (= m/4) is assigned to both parts of it. The fixed-base frequency and the damping ratio of the structure without the base isolation equal 4 Hz and 0.07, respectively. The nonlinear isolation mechanism acting in the horizontal direction and located between the upper and lower basemats consists of Neoprene pads, resulting in a frequency of 1 Hz, and friction plates with a coefficient of 0.17. The following parameters apply: $a/c_s = 0.06$, $h/a = 1.5$, $m/(\rho a^3) = 3$ (ρ = mass density of soil). Horizontal and vertical artificial time histories which follow the US-NRC response spectra, both normalized to 0.21 g, are used. The soil is modeled as a halfspace with $\bar{\zeta}_v = 0$ (Fig.4) and also as a layer built-in at its base with the depth equal to the radius and $\bar{\zeta}_v = 0.02$ (Fig.5).

	Without Base Isolation				With Base Isolation	
	Halfspace		Layer		Halfspace	
	Convolution Integral	Spring and Dashpot	Convolution Integral	Spring and Dashpot	Convolution Integral	Spring and Dashpot
Horizontal at Top	0.415	0.360	0.860	0.511	0.189	0.188
Horizontal at Upper Basemat	0.245	0.234	0.240	0.247	0.251	0.223
Horizontal at Lower Basemat	0.245	0.234	0.240	0.247	0.271	0.284
Vertical	0.273	0.262	0.498	0.315	0.273	0.262

Table 1: Maximum Total Acceleration [g]

Calculations are performed not only with the rigorous procedure based on the convolution integral but also approximately, using springs and dashpots to represent the soil. The static-spring coefficient and the damping coefficient for high frequency are used. As is visible from Table 1 for the (linear) structure without base isolation, the approximate method works better for the halfspace than for the layer, as, in the latter case, the dynamic-stiffness coefficients depend strongly on the frequency. Another choice of the frequency-independent coefficients of the spring and dashpots, e.g. evaluated at the fundamental frequencies, would result in a better agreement. For the nonlinear case, the two procedure lead to similar results, as the influence of the soil is diminished for a structure with base isolation.

STRUCTURE WITH PARTIAL BASEMAT UPLIFT

To be able to model the variable contact area between the soil and the basemat, the interface has to be discretized into boundary elements, shown in Fig.10 as squares. The corresponding flexibility matrix $[F^g_{bb}(t)]$ is calculated from the vertical influence function at the free surface of the undamped halfspace $\bar{w}(tc_s/r)$ for a unit-impulse point force. The vertical displacement at distance r from the applied load P follows as

$$w(r,t) = \frac{P_s c}{G r^2} \bar{w}\left(\frac{t_s c}{r}\right) \qquad (24)$$

In Fig.7, $\bar{w}$ is plotted, whereby the temporal variation of the point force is approximated by a Gaussian distribution with the parameter compatible with the time step Δt of the explicit integration (Eq. 22).

As a check, the vertical displacement of a rigid circular basemat for a unit-impulse force is calculated using $\bar{w}$ based on the discretization shown in Fig.10, assuming relaxed contact. In this procedure, the compatibility and equilibrium equations are formulated in the time domain. This vertical flexibility (Fig.8) agrees well with that calculated from the flexibility in the frequency domain of the total basemat (Fig.4b).

The structure (described in Fig.6) without base isolation is excited by the horizontal earthquake normalized to 0.4 g and the vertical one (0.267 g). The parameters are the same as described in the previous section. For this level of acceleration, the basemat will partially lose contact with the soil (uplift, Refs. 8,9). Slipping is disregarded.

No uplift occurs during the first second of the time history. The time histories of the vertical soil reaction and of the overturning moment during the following 1.5 s are plotted in Fig.9. Compared to the linear analysis, a significant increase of the vertical reaction occurs, leading to high-frequency oscillations. The elevation of the basemat and the vertical soil pressure shortly after uplift has started are plotted in Fig.10.

Acknowledgment

The computer center of FIDES in Zürich donated the computer time, which is gratefully acknowledged.

REFERENCES

1 J.P. Wolf, 'Dynamic Soil-Structure Interaction', Prentice-Hall, Englewood Cliffs, N.J. (1985).

2 J.P. Wolf, P. Obernhuber, B. Weber, 'Response of a Nuclear-Power Plant on Aseismic Bearings to Horizontally Propagating Waves', Earthqu. Engng Struct. Dyn., Vol.11 (1983), 483-499 .

3 A.S. Veletsos, B. Verbic, 'Basic Response Functions for Elastic Foundations', J. Engng Mech. Div., ASCE, Vol.100, April(1974), 189-202.

4 J.P. Wolf, B. Weber, 'On Calculating the Dynamic-Stiffness Matrix of the Unbounded Soil by Cloning', Int. Symp. Num. Models in Geomechanics, Zurich, Sept. 13-17 (1982), A.A. Balkema, Rotterdam, 486-494.

5 J.P. Wolf and G.R. Darbre, 'Dynamic-Stiffness Matrix of Surface Foundation on Layered Halfspace based on Stiffness-Matrix Approach', in summary report of IAEA specialists' meeting on 'Gas-Cooled Reactor Seismic-Design Problems and Solutions' held at General Atomic Company, San Diego, CA, USA, August 1982, GA-A17034, IAEA No. IWGGCR/6, UC-77 (1983).

6 J.P. Wolf and G.R. Darbre, 'Dynamic-Stiffness Matrix of Embedded and Pile Foundations by Indirect Boundary-Element Method', Trans. of the 7th Int. Conf. on Struct. Mech. in Reactor Technology, Chicago, 1983, Paper K11/1.

7 G.N. Bycroft, 'Soil-Structure Interaction at Higher-Frequency Factors', Earthqu. Engng Struct. Dyn., Vol.5 (1977), 235-248.

8 J.P. Wolf, 'Soil-Structure Interaction with Separation of Base Mat from Soil (Lifting-Off)', Nucl. Engng Design, Vol.38 (1976), 357-384.

9 J.P. Wolf, P. Obernhuber, 'Response of Structures Permitting Lift-Off to Rotational Input Motion from Horizontally Propagating Waves', 2nd ASCE Conf. on Civil Engng and Nucl. Power, Knoxville, TE, USA, Sept. 1980, Vol.VI, Paper 4-2.

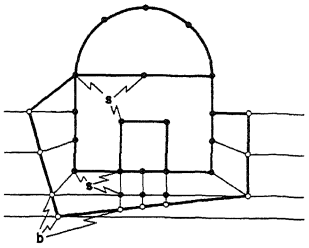

Fig.1 Structure-Soil System with Irregular Soil Region

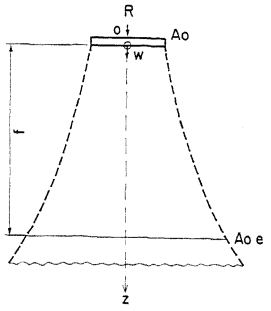

Fig.2 Semi-infinite Rod with Exponentially Increasing Area

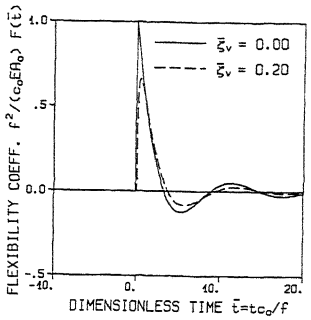

Fig.3 Dynamic Flexibility in Time Domain, Rod with Exponentially Increasing Area

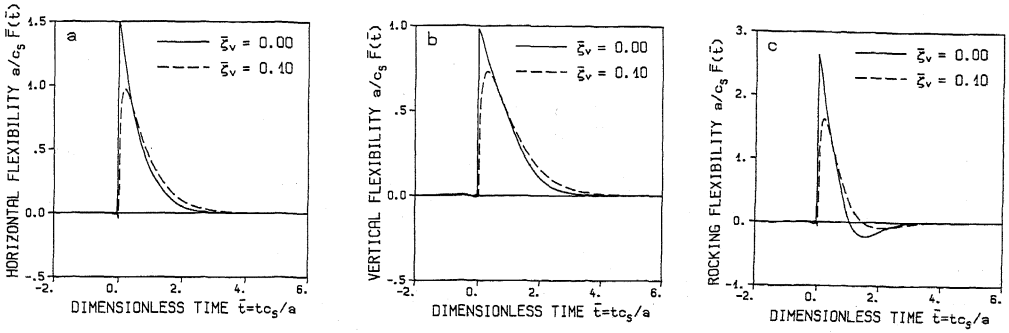

Fig.4 Dynamic Flexibility in Time Domain, Halfspace

a) Horizontal (Factor $\frac{2-\nu}{8Ga}$) b) Vertical (Factor $\frac{1-\nu}{4Ga}$) c) Rocking (Factor $\frac{3(1-\nu)}{8Ga^3}$)

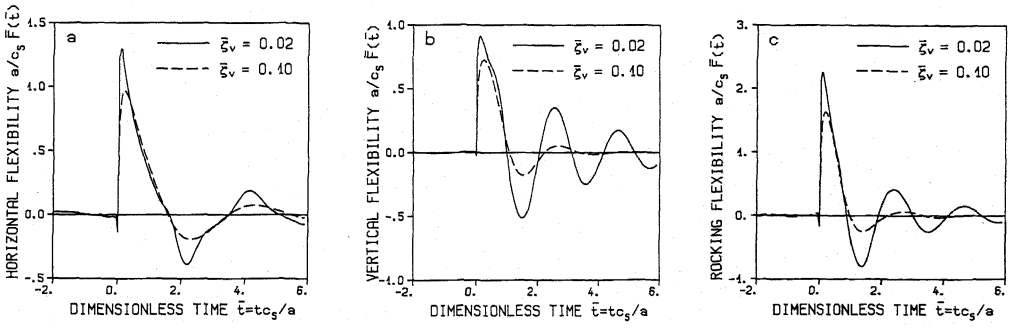

Fig.5 Dynamic Flexibility in Time Domain, Layer Built-in

a) Horizontal (Factor $\frac{2-\nu}{8Ga}$) b) Vertical (Factor $\frac{1-\nu}{4Ga}$) c) Rocking (Factor $\frac{3(1-\nu)}{8Ga^3}$)

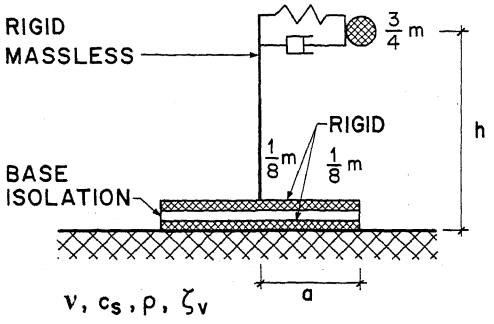

Fig.6 Model of Investigated Structure

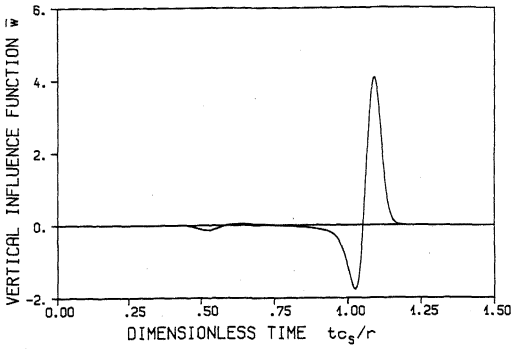

Fig.7 Vertical Displacement at Surface of Halfspace from Point Load

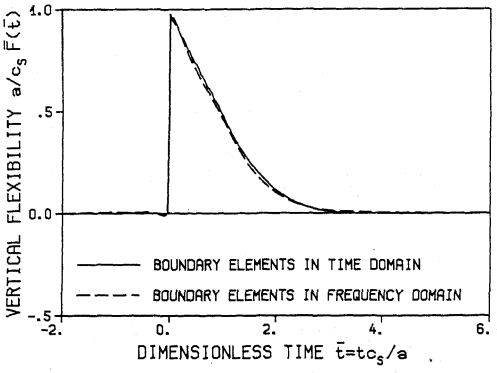

Fig.8 Comparison of Calculation Procedure, Halfspace without Damping (Factor $(1-\nu)/(4Ga)$)

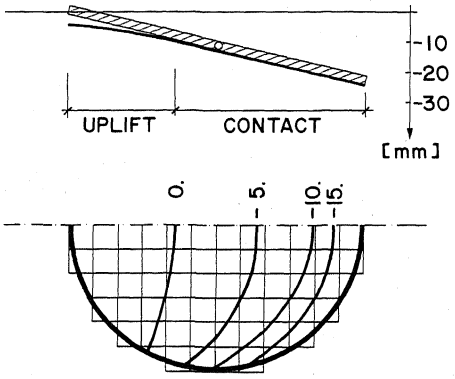

Fig.10 Elevation of Basemat and Vertical Soil Pressure ($[m/s^2]$, Factor ρa) at t = 1.10 s

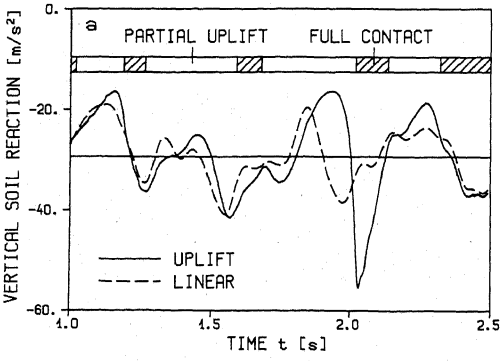

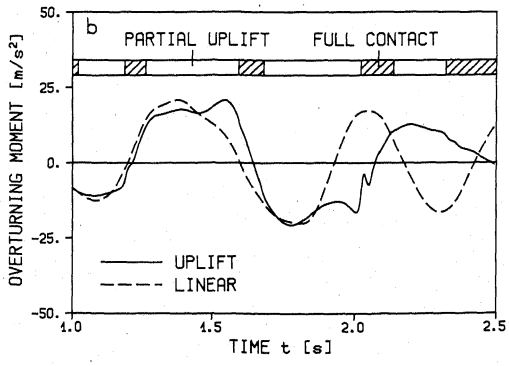

Fig.9 Time History of Total Soil Reaction
a) Vertical Force (Factor ρa^3) b) Overturning Moment (Factor ρa^4)